

Article

Forecasting of Future Flooding and Risk Assessment under CMIP6 Climate Projection in Neuse River, North Carolina

Indira Pokhrel ¹, Ajay Kalra ^{1,*} , Md Mafuzur Rahaman ² and Ranjeet Thakali ³

¹ School of Civil, Environmental and Infrastructure Engineering, Southern Illinois University, 1230 Lincoln Drive, Carbondale, IL 62901-6603, USA; indira.pokhrel@siu.edu

² AECOM, 2380 McGee St Suite 200, Kansas City, MO 64108, USA; mafuzur.rahaman@aecom.com

³ Bayer-Risse Engineering, Inc., 78 State Highway 173 W, Suite#6, Hampton, NJ 08827, USA; rthakali@bayer-risse.com

* Correspondence: kalraa@siu.edu; Tel.: +1-(618)-453-7008

Received: 7 July 2020; Accepted: 18 August 2020; Published: 28 August 2020



Abstract: Hydrological extremes associated with climate change are becoming an increasing concern all over the world. Frequent flooding, one of the extremes, needs to be analyzed while considering climate change to mitigate flood risk. This study forecast streamflow and evaluate risk of flooding in the Neuse River, North Carolina considering future climatic scenarios, and comparing them with an existing Federal Emergency Management Agency study. The cumulative distribution function transformation method was adopted for bias correction to reduce the uncertainty present in the Coupled Model Intercomparison Project Phase 6 (CMIP6) streamflow data. To calculate 100-year and 500-year flood discharges, the Generalized Extreme Value (L-Moment) was utilized on bias-corrected multimodel ensemble data with different climate projections. Out of all projections, shared socio-economic pathways (SSP5-8.5) exhibited the maximum design streamflow, which was routed through a hydraulic model, the Hydrological Engineering Center's River Analysis System (HEC-RAS), to generate flood inundation and risk maps. The result indicates an increase in flood inundation extent compared to the existing study, depicting a higher flood hazard and risk in the future. This study highlights the importance of forecasting future flood risk and utilizing the projected climate data to obtain essential information to determine effective strategic plans for future floodplain management.

Keywords: streamflow; CMIP6; bias correction; HEC-RAS; flood inundation maps; risk assessment

1. Introduction

According to the Intergovernmental Panel on Climate Change (IPCC) report, climate change has triggered extreme hydrologic events that are having adverse effect on the hydrological cycle and human livelihoods all over the world [1]. In addition, climate change plays a vital role in the ecosystem shift, leading to an increase in global warming [2,3]. Moreover, greenhouse gas emissions (GHG), induced by anthropogenic factors, are escalating the rate of global warming. If the rate of GHG emissions continues to increase at the same rate as today, others predict global warming to increase from 1.5 to 2 °C by 2052 [1]. The rising trend in global warming maximizes the evaporation rate of surface water and soil moisture that will affect the amount of precipitation all around the globe [4]. This type of alteration in the hydrologic cycle will affect the runoff and availability of both the surface and subsurface water, which eventually impacts river streamflow [5]. Furthermore, the regional precipitation trend will be affected by the patterns of ocean currents and wind, which will ultimately result in a change in streamflow. Subsequently, high flows and low flows i.e., floods and droughts, are likely to occur more

frequently across the globe with increased intensity [6–8]. These increases in both high and low flow extremes have already occurred in some parts of the world and are making societal infrastructure more sensitive to climate change [3]. Moreover, extreme events are more frequent these days and are anticipated to continue at the same frequency or even faster in the future.

Flooding is one of the most frequently occurring natural hazards in the world, along with droughts and heatwaves [7,8]. Due to the changing intensity and frequency of extreme rainfall, different parts of the world are facing deadly flood events causing a significant loss of life and property [9]. Some studies [7,10] analyze the potential impact of climate change and flood risk on a global scale, where they discuss the change in flood frequency and its impact on population centers in different parts of the world. In the United States, various studies [11–13] evaluated the change in regional streamflow due to the changes in climate. Arnell et al. [14] showed that the alterations in annual precipitation distribution in North Carolina (NC) with the warming climate might increase extreme flooding events and water quality problems in the future. Moreover, global warming is a threatening issue for a coastal state like NC. As per the IPCC [1], rising sea levels due to global climate change pose a high risk for coastal communities and low-lying areas, as there will be a higher possibility of consequences such as high tides, storms, and flooding. Johnson et al. [12] predicted, under different future climate change scenarios, that the Neuse River Basin (NRB) in NC will experience an increase in streamflow due to the increase in rainfall intensity. In recent years, NRB has endured deadly flood hazards due to heavy rainfalls resulted in from hurricanes Matthew in 2016 and Florence in 2018. Hall [15] estimated annual losses of USD 54 billion across the United States due to the extreme flooding events induced by the hurricane and tropical storms [15]. The National Flood Insurance Program was established in the United States in 1968 and managed by the Federal Emergency Management Agency (FEMA) to provide quick response to reduce the impact of flooding. Flood mapping is one of many programs organized by FEMA in various areas that are more vulnerable to flooding in the USA. FEMA utilizes software such as the HEC-RAS, to perform one-dimensional (1D) hydraulic modeling for the generation of flood inundation maps, which can also be used for flood risk analysis and insurance programs [16].

HEC-RAS, a hydraulic analysis program, was developed by the US Army Corps of Engineers in 1995 to work in a network that would support multi-user and multi-tasking environments. HEC-RAS helps to simulate water surface profiles for steady and unsteady flow, water quality analysis, and sediment transport computation, utilizing a graphical User Interface for interaction with the system [17,18]. Additionally, using the RAS Mapper, HEC-RAS can generate inundation maps and analyze flood patterns. The outcome of HEC-RAS simulation can be used for floodplain mapping, management, and insurance studies. Many researchers have applied the HEC-RAS 1D steady analysis for the simulation of a floodplain flows [19–23]. Some researchers extended the study to the hazard, vulnerability, and risk assessment of floodplains using geographic information systems, concluding that this is an important step for flood risk management [24–28]. Tingsanchali and Karim [25] deduced that the impact of future flooding could be identified using a risk assessment to mitigate human losses and attenuate economic as well as environmental losses. Thus, flood hazards, vulnerability, and risk assessments provide a framework for the management of flood risk. Furthermore, Noren et al. [29] suggested that a risk assessment is a vital step in effective flood risk management for a sustainable livelihood and agricultural system management. The risk zone maps can be used as source information to prepare emergency response plans, flood management and prevention programs, and infrastructure design. The current study provides risk analysis and mapping to improve early responses to future floods.

The Coupled Model Intercomparison Project (CMIP) was started in 1995 under the World Climate Research Program to evaluate the change in the climate from past to future in the multimodel context alongside the change in radioactive forcing and natural, unforced variability [30,31]. The CMIP helps researchers and policymakers to access the impact of climate change on hydro-climatological variables such as precipitation, temperature, and streamflow using different climate projections [31]. In the sixth phase of CMIP, CMIP6, climate projections were driven by scenarios based on shared socio-economic pathways (SSP). The SSPs are updated and revised versions of representative concentration pathways

(RCPs) [32], which include anthropogenic drivers such as future emissions and land use, along with socio-economic development [33,34]. Hence, in ScenarioMIP, the primary activity of CMIP6, updated scenarios share a matrix of SSP and RCPs as an SSP_{x-y} , in which x represents the specific SSP and y represents the forcing pathways from RCP. In CMIP6 climate models, based on the observation data, and historical Atmosphere–Ocean Coupled General Circulation Model (AOGCM) data obtained from different global climate models (GCMs) used future climate projections for different scenarios [32]. GCMs provide the resources to understand potential changes in regional and global climates [35–37]. Since the ensemble climate projection data improve the uncertainty and model biases, the literature recommends that there are at least two or more GCMs and multi-members of the GCMs for a multimodel ensemble to investigate the impact of future extremes [38–42]. Different GCMs were utilized by numerous studies [6,7,43] to discuss the various climate change simulations, considering the extreme daily precipitation and temperature. However, there are limited studies [8,11,44] related to the future projection of streamflow. For different recurrence intervals, the future streamflow was estimated in the current study utilizing CMIP6 streamflow projections from multiple GCMs.

GCMs of different climate projections encompass different systematic error and uncertainty factors called biases, which need to be corrected to rectify the over- or underestimated results [43,45,46]. Different studies have suggested different bias correction techniques to maintain consistency in future projection and reduce the error in GCMs outputs that would help to analyze the impact of climate change [47–53]. A cumulative distribution function- transformation (CDF-t) bias correction technique was developed by Michelangeli as the extension of quantile-matching that directly deals with and provide CDFs [50,51]. The theory of CDF-t assumes that the translation of CDF of GCMs variables is only possible where the transformation function exists [52]. It was utilized by many researchers to effectively reduce the bias for the given large-scale future hydroclimatic data [50–53]. Furthermore, Yuan and Wood [54] concluded that bias correction of streamflow was more efficient and reliable for ensemble forecasts. In the current study, bias-corrected multimodel GCMs is employed for the evaluation of peak discharge events.

Among the different probability distributions in the past studies [44,55–58], Generalized Extreme Value (GEV) was considered as a more efficient and better fit for the streamflow distribution. GEV is also used as a statistical best fit distribution to predict future extremes, especially hydroclimatic extremes by several researchers [55,59]. GEV is a parametric distribution, which utilizes shape, location, and scale parameters to find the cumulative probability for the given event [60]. Previous studies by Hosking and Wallis [60,61] suggested L-moment as one of the methods that was widely used for the estimation of the three parameters used in this distribution. GEV is commonly used in the streamflow distribution of the humid subtropical regions [59,62–64]. Additionally, in the current study, GEV was employed for the estimation of design flows at different recurrence intervals. The study methodology further uses the peak annual streamflow obtained from GEV to predict future streamflow. This study also utilized the quantified flows in the hydraulic model simulation. The hydraulic simulation is used to forecast the extent of the floodplains in the future climate, which is further used for the future flood risk assessment.

The objective of the current study is to forecast the future design discharge and floodplain inundation extent to access the future flood risk imposed upon the Neuse River in NC. The novelty of the study is forecasting the extent of the floodplain and assessment of the risk of the flooding in future climate using the streamflow projection data, that are made available under CMIP6. This study also compared the future and existing FEMA flooding scenarios with the calculated future design discharge to understand the increased severity of flooding in future years. Two design discharges, a 100-year return period and a 500-year return period were used in the 1D hydraulic modeling simulation using HEC-RAS to produce flood inundation maps. Moreover, this study evaluates the difference in the extent of historic flooding with the projected future flooding under the changing climate. The hazard assessment and vulnerability assessment were employed to analyze the anticipated flood risk and help shed light on the severity of risk within the study area. Finally, the risk zone mapping was performed

using the projected design discharges. The result obtained from this research might be beneficial for responding to the following questions:

- (a) What would be the impact of climate change on future streamflow, and how will it affect the flood frequency?
- (b) Under the projected design discharge, what would be the future change in flood extent and patterns?
- (c) By what times would the future flood risk increase under the climate change scenarios compared to existing FEMA scenario?

This study forecasted the future floodplain inundation area. It assessed the future flood risk to determine the extent of flood-affected urban and agricultural areas due to increasing streamflow. The outcome of this study will enable policymakers to employ better water resources management measures and lower the risk under the future climate.

2. Study Area and Data Used

2.1. Study Area

The study area was selected in a reach of Neuse River that originates from the confluence Eno and Flat River at Durham County, NC. The Neuse River flows toward the southeast United States in between the piedmont and Pamlico Sound [65,66]. The study reach is 32 km long, and extends from a latitude and longitude of 35.23° N, 77.77° W at the river's upstream with an elevation of 10.73 m to latitude and longitude of 35.25° N, 77.58° W at the river's downstream with an elevation of 4.15 m. The United States geological survey (USGS) gauge station at Neuse River, Kinston (Station ID 02089500) is located 1.2 km upstream from the downstream end of the study reach at the elevation of 3.3 m above NGVD29. The agricultural land, residential area, and wetlands dominate the study reach. The city of Kinston is the principal city within the study area, as shown in Figure 1a,b. This city has experienced numerous flooding events in the past due to extreme rainfall. The study area is a humid subtropical climate with the highest temperature in July and maximum rainfall in September with the average annual precipitation of 1235.96 mm [67]. In the past, this region suffered many extreme flood events due to higher category hurricanes such as hurricane Hazel, Fran, Floyd, and Matthews. Recently, in 2018 hurricane Florence made a devastating impact in the city of Kinston due to storm surge with a record-breaking gage height for that area along with landfall in a different area of NC [68]. The selected reach, Neuse River, along with the city of Kinston, is located in Lenoir County, NC, as shown in Figure 1b. This study used the existing information of the study area from a FEMA flood insurance study (FIS) report [69], hereafter referred to as FFR within this article. Figure 1c shows the digital elevation map (DEM) with the elevation information of the study reach along with the FFR assigned cross-sections.

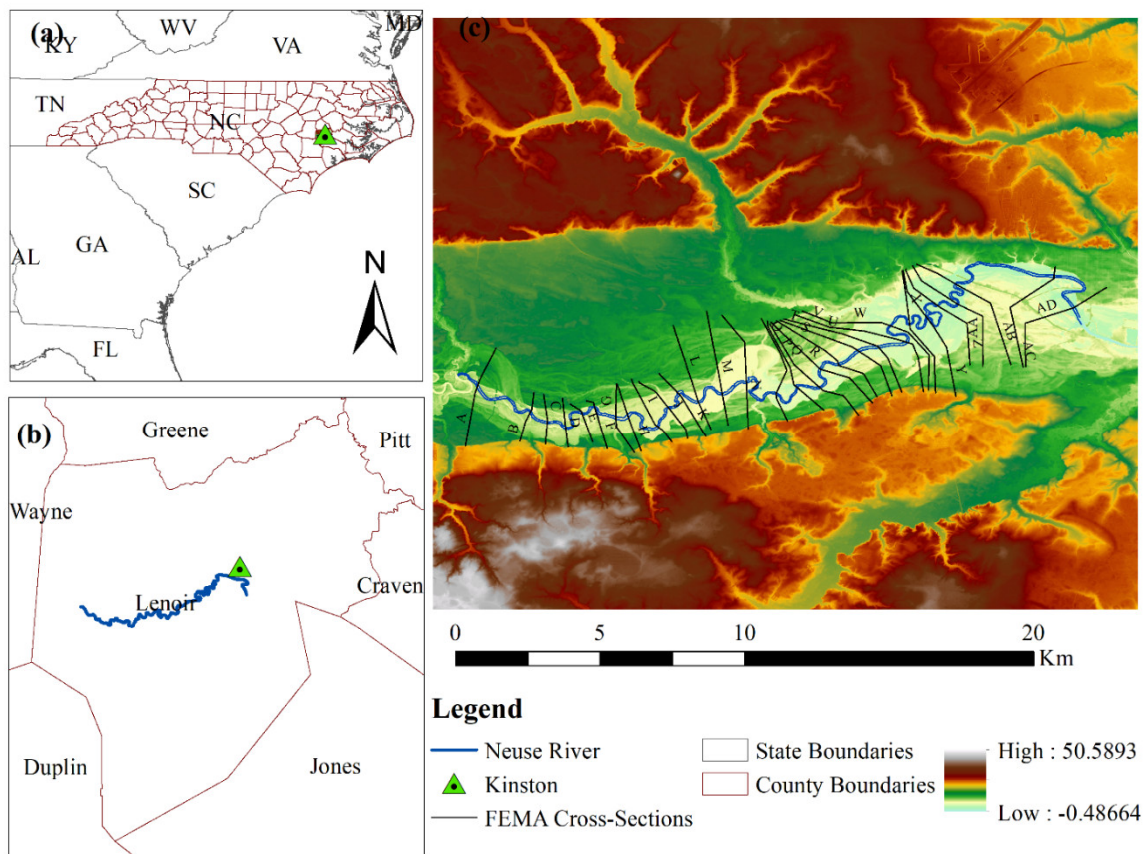


Figure 1. Study area: (a) States boundaries outlining counties of North Carolina (NC) including Kinston City, (b) Lenoir county showing the Kinston City at downstream of the study reach, (c) existing information of the study area from a FEMA flood insurance study (FIS) report (FFR) cross-sections and their labels along with their elevation.

2.2. Dataset

Using single GCM can have more uncertainties in the results [49], so this study utilizes scenarios of CMIP6 consisting of two or more GCMs. Specifically, this study uses four scenarios among twelve available scenarios. Eight scenarios were eliminated due to having only one GCM, and daily streamflow data from selected scenarios are used to evaluate the peak streamflow of the study reach. In CMIP6-AOGCMs, three GCMs for the historic year were available with several climatic projections which were obtained from the model institute named Centre National de Recherches Meteorologiques/Centre Europeen de Recherche et Formation Avancees en Calcul Scientifique (CNRM-CERFACS). A long modeling period from 1950 to 2014 is taken as a historic period. For future streamflow datasets, four different scenarios i.e., SSP1-2.6, SSP2-4.5, SSP3-7.0, and SSP5-8.5, each having two different GCMs from 2036 to 2100 are utilized to access the impact of a hydroclimatic variable in future. These four different future scenarios include climate-changing anthropogenic factors, along with the socio-economic developments [34]. Table 1 presents the scenarios used in this research along with the number of ensemble members. The historical observation data are extracted from the USGS gauge station 02089500, from 1950 to 2014. Also, the gridded streamflow data from CMIP6 has centroid near this USGS gauge station.

Table 1. Global climate models' (GCMs') historical and future scenarios used in the study along with their number of ensemble members and modeling institute [70].

Scenarios	Model Name			Modeling Institute
	CNRM-CM6	CNRM-ESM2	CNRM-CM6-HR	
Historical	√ (24)	√ (5)	√ (1)	CNRM-CFRFACS
SSP5-8.5	√ (5)	√ (6)		CNRM-CFRFACS
SSP3-7.0	√ (5)	√ (6)		CNRM-CFRFACS
SSP2-4.5	√ (5)	√ (6)		CNRM-CFRFACS
SSP1-2.6	√ (5)	√ (6)		CNRM-CFRFACS

The USGS national map viewer provides the DEM (<https://viewer.nationalmap.gov/basic/>). For a model with higher accuracy, the literature suggests finer resolution DEM [23,71]. However, due to the limitation of available data, this study used 10-m resolution DEM. Figure 1 shows the DEM of the study reach showing the elevation along with the FFR assigned cross-sections. The land use and land cover data were obtained from the website of Multi-Resolution Land Characteristics Consortium (MRLC) [72] provided the land use and land cover data, which provides the Manning's roughness coefficient of different land use. In this study, the most recent National Land Cover Dataset (NLCD) 2016 data were used. The location of the river cross-sections was selected in and between the cross-section assigned by FFR to aid in the calibration of the hydraulic model. Since the detail of structures like dams, the levee location elevations were not readily available, they were not considered in this study. Furthermore, Manning's values were adopted from FFR for the selected reach length of the Neuse River. FEMA developed a hydraulic analysis flood along with the prediction of different year recurrence flows. Since FEMA performs the flood frequency analysis based on a 100-year and 500-year return period, this study followed the same course, i.e., 100-year (0.1% chance) and 500-year (0.2% chance) of annual occurrence of flooding events. Table 2 shows the extreme streamflow discharges obtained from FFR near Kinston City, NC for the Neuse River.

Table 2. Summary of discharge (m^3/s) at USGS gage site 02089500, downstream of study reach given by FFR [69].

Flooding Source	Location	Drainage Area (Sq. Km)	10% Annual Chance (m^3/s)	2% Annual Chance (m^3/s)	1% Annual Chance (m^3/s)	0.2% Annual Chance (m^3/s)
Neuse River	Approximately 1.2 km upstream of the confluence of Adkin branch	6972.25	639.96	982.59	1146.83	1574.42

3. Methods

The methods section is divided into two sub-sections. First, it explains the statistical analysis to predict future design discharge. Secondly, it depicts a detailed guideline of hydraulic analysis to generate the flood inundation maps and further assessment of potential hazard, vulnerability, and risk. Figure 2 presents the steps involved in this study as the flowchart, which are further discussed below in a sequential manner.

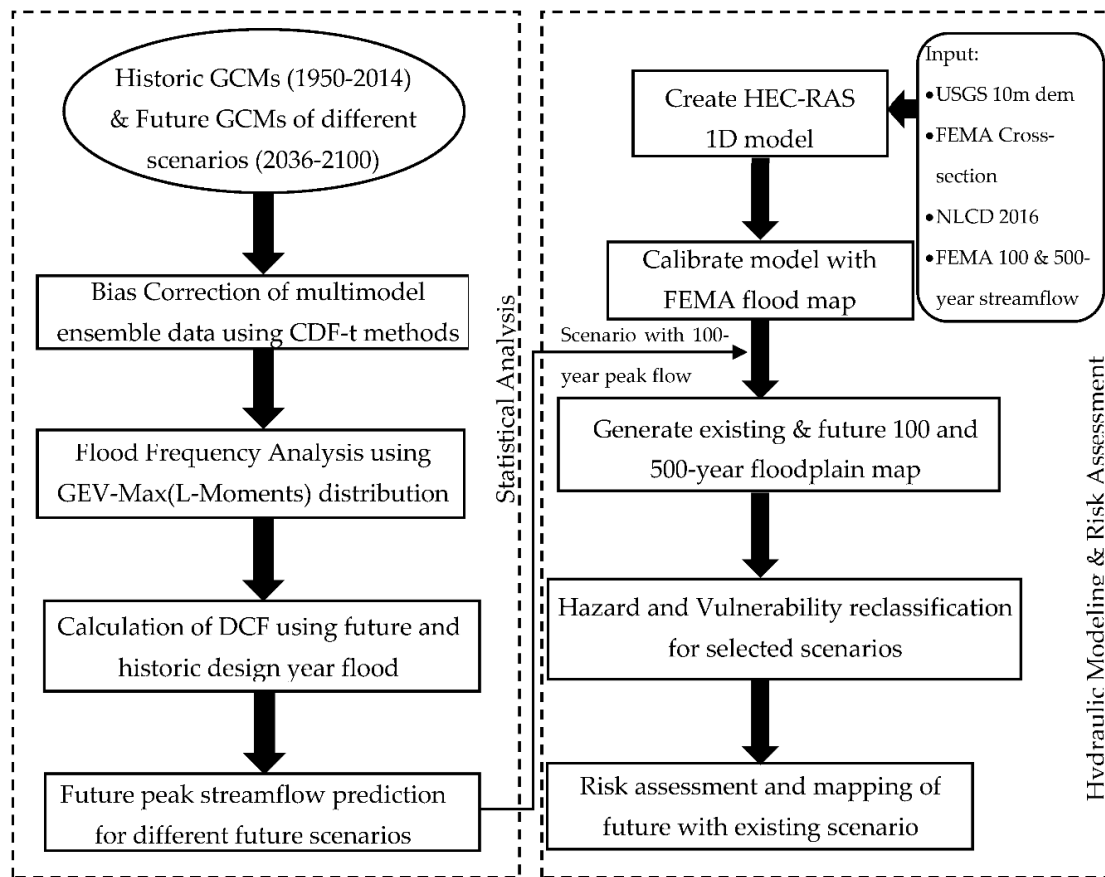


Figure 2. Schematic diagram showing the sequential steps followed to analyze flood frequency, predict the future streamflow, flow routing, floodplain mapping, and risk assessment.

3.1. Statistical Analysis

The following two sub-subsections discuss the statistical analysis involves bias correction of CMIP6 streamflow data and quantification of the future design flows.

3.1.1. Bias Correction

The streamflow data obtained from CMIP6 consist of significant systematic biases, that requires bias correction before further application. Moreover, before bias correction, an ensemble of GCMs was performed for each of the scenarios, so that it would increase the robustness in predicting future change [38,40,73]. In this study, the CDF-t method was chosen for the bias correction of multimodel ensemble CMIP6 streamflow data [50–53]. The CDF-t method develops the relationship between modeled and observed CDF outputs, considering the transformation function “T”, where daily observed data were utilized [51]. The descriptive figure to describe the CDF-t methods is as shown in Figure 3, where the modeled future (F_{gf}) and historical climate data (F_{gh}) along with historical observed historical data (F_{sh}) have been used to obtain future bias-corrected data (F_{sf}). Figure 3 shows the F_{sf} as the green dotted line. The bias-corrected value of F_{gh} should fall within the range of F_{sh} . All three arrows, a, b, and c showed the sequential steps of bias correction. Since it is impossible to plot the future change beyond the maximum F_{sh} , arrow “b” moves right toward arrow “c” to intersect the green dot line, which finally generates the bias-corrected data.

The following develops the series of the equation used for the bias correction starting with:

$$T(F_{Gh}(x)) = F_{sh}(x) \tag{1}$$

Let us consider, $u = F_{Gh}(x)$, that gives us $x = F_{Gh}^{-1}(u)$, where $u \in [0, 1]$.

Then, Equation (1) is transformed to

$$T(u) = F_{sh}(F_{Gh}^{-1}(u)) \tag{2}$$

where T represents the functional relationship between the modeled and observed CDF results concerning the historical period.

Validating the Equation (2), the final CDF-t equation is:

$$F_{sf}(x) = F_{sh}(F_{Gh}^{-1}(F_{Gf}(x))) \tag{3}$$

Here, the functional relation is established between observed and modeled streamflow for historical data to be utilized for future periods. Furthermore, the utilization of modeled projection and estimating the CDF of future climate projection is performed, and hence, the bias-corrected data is used for the prediction of future flow.

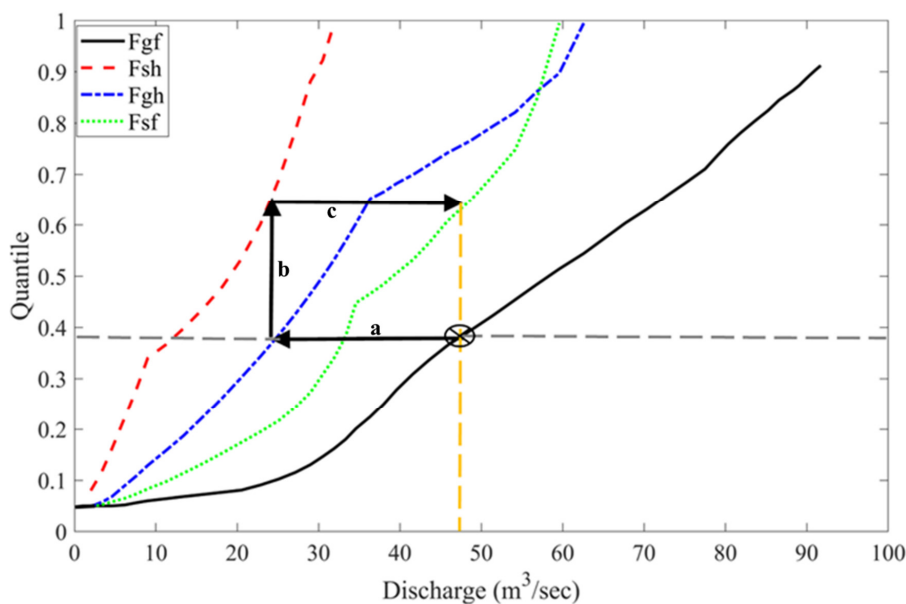


Figure 3. Illustrative figure showing bias correction using CDF-t methods.

3.1.2. Quantification of the Future Design Flow

After the bias correction of streamflow data, the next step is to calculate future design flow. Annual peak streamflow is extracted from each multimodel ensemble scenario (SSP5-8.5, 3-7.0, 2-4.5, 1-2.6) for future time series of 2036 to 2100. Annual peak flow is also calculated for the observed historical time series of 1950 to 2014, from the same USGS gauge station as an earlier step. Then GEV probability distribution is utilized to analyze the annual maximum flow for different recurrence intervals. The equation that was used by the GEV distribution for the annual maxima is given below.

$$GEV(x : \mu, \sigma, \kappa) = \begin{cases} \exp \{ - [1 + \kappa (\frac{x-\mu}{\sigma})]^{-1/\kappa} \} & \text{if } \kappa \neq 0 \\ \exp \{ - \exp [- (\frac{x-\mu}{\sigma})] \} & \text{if } \kappa = 0 \end{cases} \tag{4}$$

In this equation, μ , σ , and κ are GEV parameters respectively representing the location, scale, and shape of the data. Additionally, for shape parameter $\kappa > 0$, $\mu - \sigma/\kappa < x < \infty$; $\kappa = 0$, $-\infty \leq x \leq \infty$; $\kappa < 0$, $-\infty \leq x \leq \mu - \sigma/\kappa$ [58]. Using L-moments, location, scale, and shape parameters are calculated to fit the GEV distribution. Thus, the obtained peak flows for different year return periods are utilized for the estimation of future peak flow. Peak flow for 100 and 500-years is calculated for both climate modeled and observed data with GEV for hydraulic analysis. After the GEV analysis, the delta change

method (DCM) is used where the delta change factor (DCF) helps to estimate a different design flood events for evaluation of future peak flows [44]. The main idea of using DCM is to match the currently observed gage streamflow data and FFR streamflow data. For individual scenarios (SSP5-8.5, 3-7.0, 2-4.5, 1-2.6), DCF is calculated and a scenario with higher DCF is chosen for further study. The selected scenario with higher DCF will exhibit an increase in future design flow in its maxima. Thus, GEV generated streamflow for 100-years and 500-year return period are multiplied by the DCF to predict future design streamflow.

3.2. Hydraulic Modeling and Risk Assessment Classification

The hydraulic modeling is performed using the 1D steady model on of HEC-RAS (version 5.0.7). The HEC-RAS model included a total of 95 cross-sections, including 30 existing from FFR to address the critical points along the reach. Manning's roughness coefficient is assigned as suggested by the FFR. The analysis uses the FFR 100-year discharge to calibrate the model with the help of the known water surface elevation levels (WSEL). The model performance is measured using different statistical measures such as Nash-Sutcliffe Efficiency (NSE), Root Mean Square Error (RMSE), Coefficient of Determination (R^2), and Percent-Bias (PBIAS) [74]. After the calibration, the model is routed for the future peak flow obtained for the "quantification of future design flow" step. Hazard and vulnerability assessments are accounted for as the vital steps in accessing the flood risk [27]. For the hazard assessment, different flood characteristics such as water velocity, water depth, and flood extent can be considered as the indicators for hazard classification. This study used water depth for the hazard assessment and attempted to classify the water depth and distinguished the hazard of that area based on the threat posed by flooding on human life. For both extreme events, 100-year, and 500-year, four hazard categories are generated [25,28]. Hazard class is divided into a low hazard (H_1), moderate hazard (H_2), high hazard (H_3), and severe hazard (H_4) class based on the critical flood depth range from 0.8 m to 3.5 m. These hazard classes along with their description are presented in Table 3. In this study, 0.8 m is considered as the level above the ground floor level and 3.5 m is considered as the roof of a single-story building for residential. The human threat is set at the ease of wading at any flooding event.

Table 3. Flood hazard classification and its description considering water depth as an indicator of the degree of hazard.

Hazards Class	Flood Depth (m)	Flood Hazard	Description of Hazard
Low Hazard	<0.8	H_1	Poses less of a hazard to people, and on-foot evacuation can be done.
Moderate Hazard	0.8–1	H_2	On-foot evacuation will be difficult and adult evacuation will be difficult. The infant will be at a serious threat.
High Hazard	1–3.5	H_3	Hazard inside house and evacuation only possible from the roof.
Severe Hazard	>3.5	H_4	All the structures will be underwater, evacuation from the roof will also be a threat as people may be drowned there too.

The Floodplain area in the Neuse River is comprised of different land-use units, which are assigned by NLCD 2016, MRLC. Based on hazard threats on the landforms, risk analysis can be done by utilizing the vulnerability. Hence, as a part of vulnerability assessment, the landforms from NLCD 2016 are reclassified into residential, forest, agriculture, wetlands, and water bodies. The residential area is assigned a value of one (1) and water a value of five (5) representing the flood risk which is lower in residential areas than in areas near the water bodies. Other classified areas such as forest, agricultural land, and wetland were assigned with values of 2, 3, and 4 values, respectively. Table 4 and Figure 4 shows the land use reclassification along with the assigned value. Previous studies showed that the vulnerabilities were assigned based on the projected flooding and socioeconomic conditions [24].

This study uses vulnerabilities based on flood hazard impact and topography for both existing and future scenarios. Furthermore, the future scenarios are comprised of socioeconomic pathways and emission scenarios, that would better depict the threat of expanding floodplains due to climate change. After that, a risk assessment is done by utilizing classified flood hazards due to flooding, which evaluates the threat posed to different landforms based on floodplain depth. Therefore, the magnitude of flood risk is reckoned as a multiplying of the flood hazard and vulnerability, which is inferred physically by assigning values on the equal interval score- a scale from 0 to 20. Scores less than zero are defined as risk free zones, Low Risk Zones are between 0 and 5, Moderate Risk Zones are between 5 and 10, High Risk Zones is between 10 and 15 and Severe Risk Zones are greater than 15 [26]. Then, the risk-map for both the 100 and 500-year design flood for future scenarios is developed. The map portrays the risk that could happen in the future in that area. Moreover, the risk map for the existing FEMA study is also developed to compare the present risk in the study area to the risk projected in the future.

Table 4. Reclassification of the land use data obtained from NLCD (2016) for the study area near Kinston with their assigned value for vulnerability assessment.

Land Classification (NLCD 2016)	Reclassification of Land Use	Score
Developed High Intensity Developed Low Intensity Developed Medium Intensity Developed Open Space	Urbanized Area	1
Deciduous Forest Evergreen Forest Mixed Forest Barren Land Grassland/Herbaceous Shrub/Scrub	Forest	2
Cultivated Crops Pasture/Hay	Agricultural Land	3
Emergent Herbaceous Wetlands Woody Wetlands	Wetlands	4
Open Water	River	5

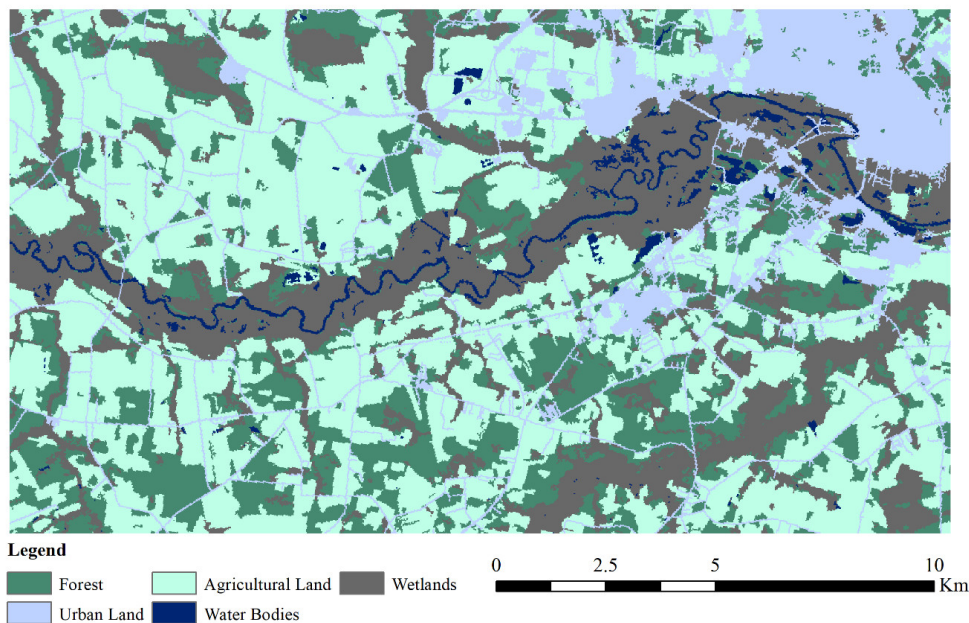


Figure 4. Reclassified NLCD map for the vulnerability assessment.

4. Results

The results are discussed in four ensuing sections. The first section discusses the bias correction results of GCMs obtained from CMIP6. This section also presents future flows that were calculated using bias-corrected data. The second section highlights the simulation results of calibrated hydraulic models that predict the extent of floodplain for different climate scenarios. The third section shows the evaluation of floodplain using classified hazard data. The final section presents the outcomes of risk analysis utilizing reclassified hazard and vulnerability data.

4.1. Flood Frequency Analysis and Performance of Hydraulic Modeling

This study uses daily streamflow data obtained from the climate model projection and USGS gage station, shown in subplots (a) and (b) of Figure 5. The data shows that the range of streamflow is increasing in the Neuse River. A total of 74 streamflow projections from 3 different GCMs of different historical and future climate data were used for the analysis of annual peak flow. The historical data helped to bias-correct future projections for each scenario from the multi-model ensemble GCMs. Figure 5b shows the annual peak flows extracted from the bias-corrected daily streamflow data for each future scenario (i.e., SSP5-8.5, 3-7.0, 2-4.5, 1-2.6). Since the study area is under the risk of catastrophic flooding, the maximum flows are analyzed in this study. Figure 5a,b shows the range of intense flows for future scenarios and historical data. The data in the different scenarios illustrate that the range of flow is greater for SSP3-7.0 and SSP5-8.5, since the projected GHG emissions are at a higher level for these scenarios in comparison to other scenarios.

For the different scenarios representing the different emission pathways, GEV-Max (L-Moments) was utilized to evaluate the design peak flows of different recurrence intervals for different future scenarios (2-year, 5-year, 10-year, 50-year, 100-year, 500-year). Considering the 100-year return period flood, the historic and future scenarios, i.e., SSP1-2.6, SSP2-4.5, SSP5-8.5 were utilized for the calculation of peak discharge, where the discharge was found to be 939.58 m³/s, 1814.93 m³/s, 1780.34 m³/s, 1917.87 m³/s, and 1921.65 m³/s, respectively. Across all four future scenarios, SSP5-8.5 generated the maximum flows as the result of higher emission scenarios producing higher radioactive forcing (i.e., 8.5 W m⁻²) by 2100. For the same scenarios, the 500-year design flow was 1283.11 m³/s, 4062.07 m³/s, 3367.09 m³/s, 3698.73 m³/s, and 3455.40 m³/s, respectively. The DCF was calculated by utilizing the different return period discharge from GEV and FFR for the Neuse River. All future return flows were divided by respective discharges according to recurrence intervals from FFR to get DCF values. Figure 5c shows the distribution of DCF for individual scenarios. From Figure 5c, it was inferred that the scenario SSP1-2.6 represents the lowest DCF, i.e., less than one, with the lowest median among all the scenarios. Moreover, scenarios SSP1-2.6, SSP2-4.5, and SSP3-7.0 have DCF values lower than the high emissions scenario SSP5-8.5. The increased value of DCF with increased emission scenarios implies that higher GHG emission, land-use change, and other integrated characteristics are likely to increase the extremes of future streamflow. The Scenario SSP5-8.5 has a higher DCF of 2.045 and 2.69 for 100-year and 500-year design floods. Later in this study, among all four scenarios, SSP5-8.5 based 100-year and 500-year design discharge are used to develop floodplain inundation maps. DCF value implies future design flows for 100-year and 500-year return periods at 2345.52 m³/s and 4239.88 m³/s, respectively. When comparing both the 100-year future and existing flow, the future flow is more than two times the existing flow. Similarly, in the case of a 500-year flow, future flow is nearly three times the existing flow. The 100-year future flow even exceeds the existing 500-year flow, demonstrating the higher flood risk in the future.

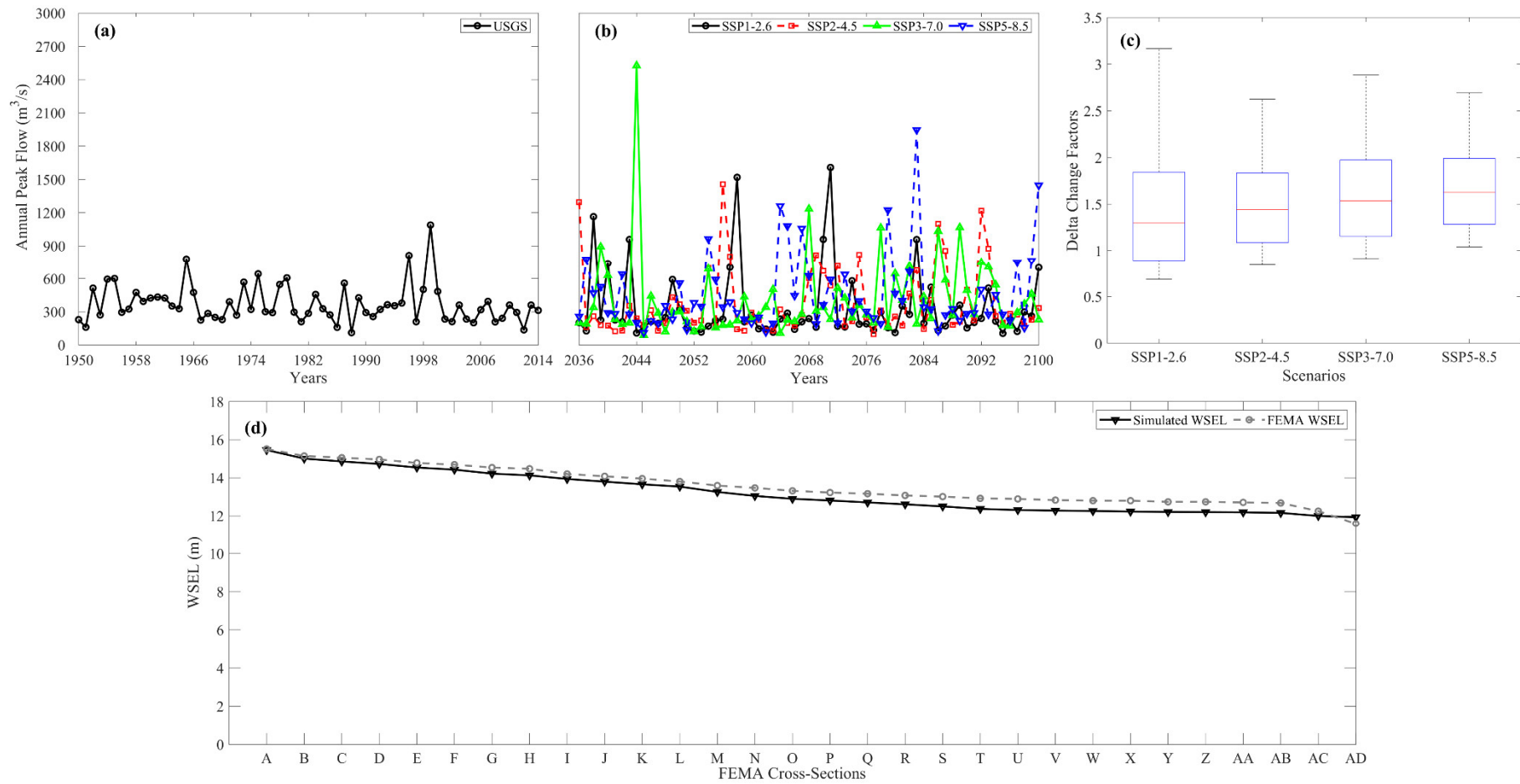


Figure 5. Annual peak streamflow for (a) historical and (b) future scenarios; (c) Box plot for the comparison of different future scenarios DCF using different recurrence intervals; (d) Calibration plot of FFR given WSEL versus Simulated WSEL.

The 1D hydraulic model was developed and calibrated using the FFR 100-year design flood. The comparison of observed and simulated WSEL was performed for the calibration using different statistical parameters. Furthermore, the WSEL for all 30 existing cross-sections from the FFR was used in the process. The Manning's "n" used were 0.05–0.06 and 0.12–0.19 for channel and floodplain respectively as suggested by FFR. Figure 5d shows the simulated and observed WSEL for the selected cross-sections. Statistical measures such as NSE, RMSE, R^2 , and PBIAS were used to calculate the robustness of the model by comparing the WSEL from the newly developed HEC-RAS model and FFR. The values of NSE, RMSE, R^2 , and PBIAS were 0.82, 0.40, 0.98, and -2.64 , respectively, and based upon the observed and simulated data. The NSE value closer to 1 suggested that the observed and simulated WSEL were closely fitted. Additionally, the RMSE value of 0.40 shows minimal error regarding observed and simulated WSEL have a close fit. The obtained R^2 value signifies that the observed and simulated WSEL are closely matched with minimal dispersion. The negative value of PBIAS illustrates the overestimation of biases. All the calculated statistical parameters were within an acceptable range and illustrated the robustness of the calibrated hydraulic model, where the predicted WSEL can be utilized to develop a floodplain inundation map.

4.2. Flood Inundation Mapping

The calibrated hydraulic model was used to generate a flood inundation map. The model used DCF implied SSP5-8.5 based future design discharge for 100-year and 500-year return period. The estimated design flows are routed in the HEC-RAS model, and the floodplain inundation areas are mapped using RAS Mapper and ArcGIS. Figure 6 shows the comparison between the floodplain inundation extent generated using the existing FEMA flows and projected future flows. Both, 100-year and 500-year floodplains for future flows are much larger than existing FEMA studies. The floodplain inundation extent generated from the 100-year flood event based on future scenarios was 1.73 times higher than the FFR 100-year floodplain inundation extent. The 500-year floodplain inundation extent was 1.68 times higher than the existing 500-year floodplain extent given by FEMA. The increased floodplain inundation area due to future streamflow that might put Kinston City in a more vulnerable situation. As a coastal state, NC has plenty of low-lying areas used for agricultural purposes [23]. Those areas might be affected due to the future changing streamflow. Additionally, the selected future scenarios, SSP5-8.5, can be used in further studies to address the significant change in streamflow linked with climate change and socio-economic change [34]. It can make a significant difference in the field of future flood studies and emergency flood management efforts.

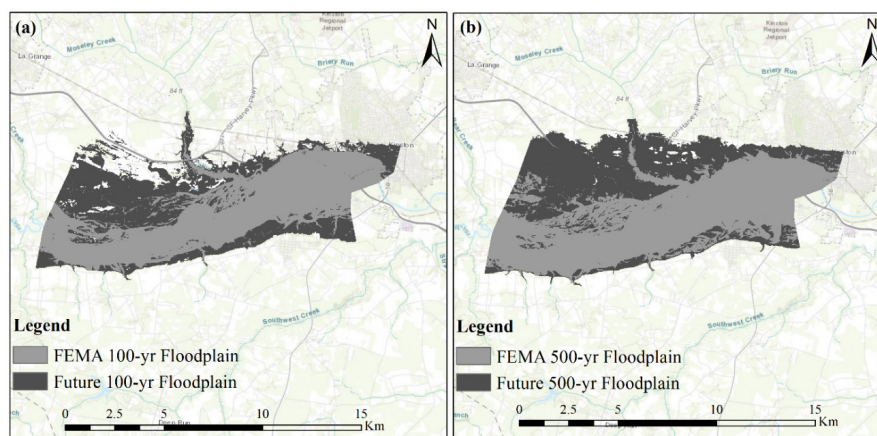


Figure 6. Comparison of flood extent map of Neuse River using the ArcMap (Version 10.7.1) between FEMA and future scenarios for (a) 100-year and (b) 500-year return period flood events, respectively. Source: Esri, HERE, Garmin, Intermap, increment P Crop., GEBCO, USGS, FAO, NPS, NRCAN, GeoBase, IGN, Kadaster NL, Ordnance Survey, Esri Japan, METI, Esri China (Hong Kong), swisstopo, © OpenStreetMap contributors, and the GIS User Community.

Many flood characteristics were obtained as an output when performing the modeling in HEC-RAS. When generating the floodplain inundation maps for different existing and future scenarios in the Neuse River top width, channel velocity, and flood extent were exported and presented in Figure 7. Figure 7 compares all the variables (top width, channel velocity, and flood extent) for the FEMA and design discharges for the existing 30 cross-sections, acquired from the FIS report, along the reach are shown in Figure 7. The projected future 100-year maximum channel velocity, computed as 1.17 m/s, is higher than the maximum channel velocity. The flood extent area for the future scenario was more than double the area for most of the cross-section in a 100-year flood and more than three times the area for the 500-year projected floodplain when compared to FEMA events. Figure 7a shows the significant changes in the top width for the channel with cross-sections B, C, D, E, F, and H for 100-year flood events. For the 500-year flood, as shown in Figure 7b, cross-sections D, E, and N showed a significant change in top width, which implies that the flood extent is higher in that area. Previous studies [24,26,44] projected 100-year flood events; however, due to this significant change in these flood characteristics in this study, this study was extended up to 500-year flood events. Including the 500-year flood events demonstrates the risk of future flooding, and can improve hydraulic structure designs to mitigate flood risk while considering climate change.

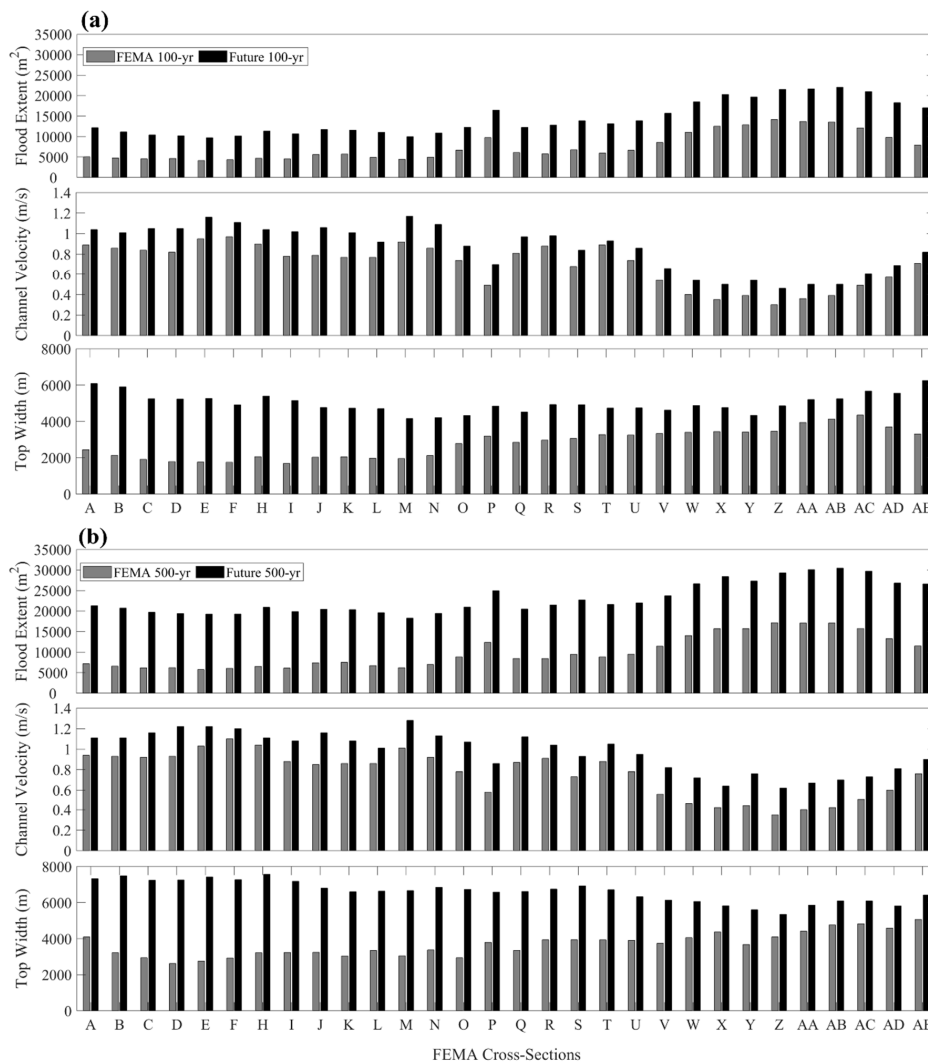


Figure 7. Comparison of flood characteristics such as flood extent, channel velocity, and top width for different flooding scenarios considering (a) 100-year and (b) 500-year return period flood events, respectively.

4.3. Flood Hazard Assessment

To assess the flood hazard, water depth was used as the quantifiable variable to study the potential threat caused due to existing FEMA and future flooding scenarios for both 100-year and 500-year design floods. All four hazard types were classified for both existing FEMA and future flood scenarios. Figure 8 presents the extent of areas covered by each hazard classification for each scenario. For the 100-year design flood, the future scenario has a higher flood hazard in comparison with the existing FEMA flooding (see Figure 8a,b). Moreover, for this flooding event, the future scenario has a larger, severe hazard floodplain and smaller moderate hazard floodplain. For both FEMA and projected scenarios, the 100-year design flood event has a severe hazard classification with 43.04% (19,219.03 km²) and 39.72% (30,766.75 km²), respectively. Since the peak flow was maximum for SSP5-8.5, there could be an increase in the floodplain inundation area with possible hazard classification as low or severe. Figure 8c,d shows the result from the analysis of a 500-year flood hazard assessment. It can be observed that the FEMA flood event has a lesser flood hazard extent than the future scenario (57,976.54 km² compared with 97,496.02 km²). Comparing the existing flood scenario with the projected scenario for 100-year and 500-year flooding events shows the extent of hazard area increased by 1.68 to 1.73 times the existing condition, respectively. The extent of 100-year and 500-year flooding increases from existing to future scenarios, demonstrating there will be potential damage in the future. Thus, these hazard areas combine with a vulnerability factor to identify the degree of risk posed within the study area.

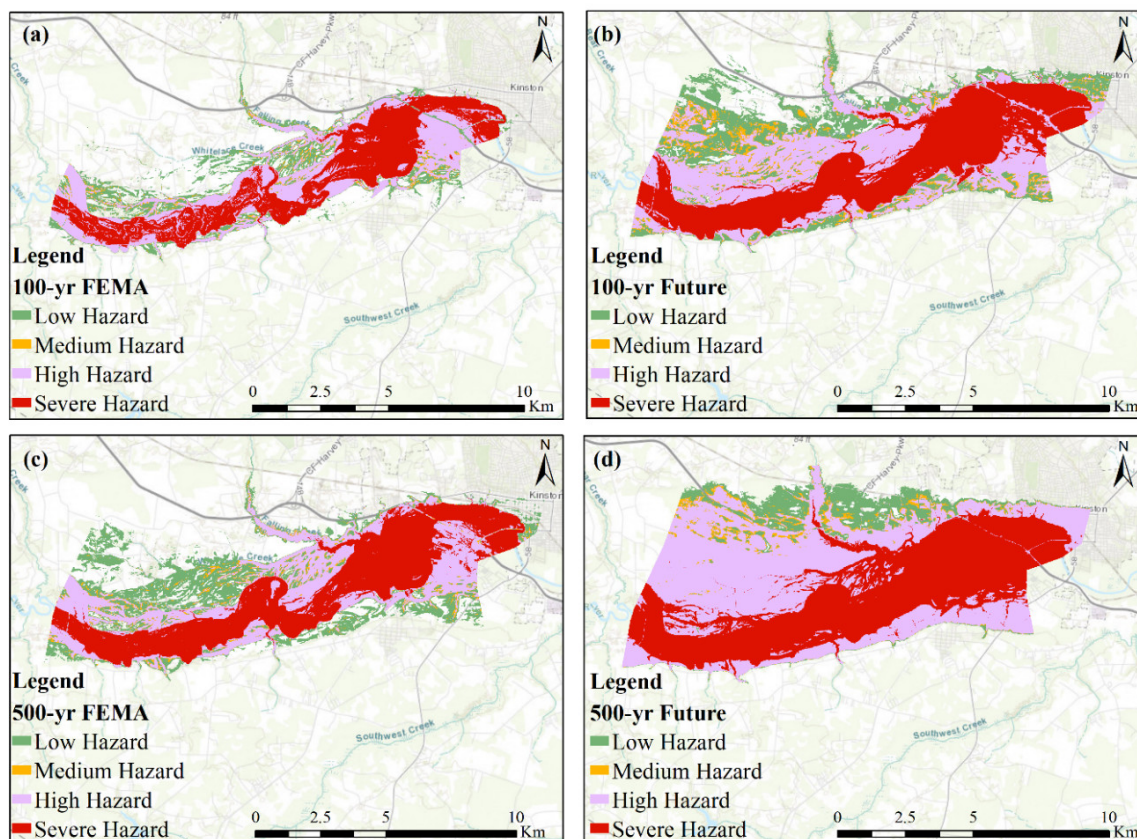


Figure 8. A Comparison of extent of flood hazard utilizing different flooding scenarios, i.e., FEMA and Future, respectively, for (a,b) 100 and (c,d) 500-year return period flood events. Source: Esri, HERE, Garmin, Intermap, increment P Crop., GEBCO, USGS, FAO, NPS, NRCAN, GeoBase, IGN, Kadaster NL, Ordnance Survey, Esri Japan, METI, Esri China (Hong Kong), swisstopo © OpenStreetMaps contributors, and the GIS User Community.

4.4. Risk Zone Assessment and Mapping

From the intersection of hazard and vulnerability map of FEMA and future climatic scenario SSP5-8.5, risk zone maps are extracted for 100-year and 500-year flooding events. Table 5 summarizes the area covered by each risk zone. The Risk Zone map is comprised of an area under the threat of possible damage [10]. For the FEMA 100-year and 500-year risk maps, a greater extent of the floodplain is covered by a severe risk zone with the area coverage of 18,644.73 km² and 23,330.17 km². For the 100-year FEMA flood, a moderate risk zone has a lower area coverage among all four risk zone with an area of 6113.23 km². Meanwhile in the 500-year flooding event, the flood coverage with high risk zone has a lower area coverage with a total area of 6044.54 km². In the future scenario, the 500-year flood moderate risk zone covers an area of 38,869.48 km² or 39.75% of the total risk area. For both the future 100-year and 500-year flooding zone, the high risk zone area covered 5211.76 km² and 8038.58 km², respectively, of the floodplain area. Moreover, Table 5 shows the 100-year and 500-year FEMA flood potential risk area to be 44,659.37 km² and 57,979.73 km², respectively. Similarly, Table 5 shows the future scenario revealed a moderate risk zone for the 100-year and 500-year return periods at 77,462.86 km² and 97,498.36 km², respectively. Additionally, it can be inferred that in contrast with the FEMA flood event, the future scenarios have a significant difference in the moderate risk zone. Furthermore, on the evaluation of 100-year and 500-year flood events, the flood risk extent of future scenarios was 1.73 and 1.68 times the existing scenarios, respectively, that shows the increasing flood risk in the future.

Table 5. Flood risk extent based on the zonal risk classification for 100-year and 500-year return period flood event for existing and future scenarios, respectively.

Risk Zone	Existing Scenario (FEMA) (km ²)		Future Scenario (SSP5-8.5) (km ²)	
	100-Year	500-Year	100-Year	500-Year
Low Risk Zone	10,468.76	18,101.99	23,773.57	21,904.91
Moderate Risk Zone	6113.23	10,503.02	22,104.30	38,869.48
High Risk Zone	9432.64	6044.54	5211.76	8038.58
Severe Risk Zone	18,644.73	23,330.17	26,373.23	28,685.39
Total	44,659.37	57,979.73	77,462.86	97,498.36

Figure 9 shows the extent of the risk zone mapped in the study area. In this study, risk zone mapping is an important factor in distinguishing the potential threat for each land use. Figure 9a shows that FEMA 100-year has a minimal threat in urbanized areas and road networks, with a larger area in the risk-free zone. The water bodies, wetlands, and forests were completely in the severe to high risk zone, which will minimize the threat to human life. Some agricultural lands are also observed to be within the low to moderate risk zone, resulting in the potential for lower crop yield during flooding events. Due to the lower elevation in the upstream side of the study area, the risk is exhibited, in contrast to the downstream part. For the 100-year future scenario (Figure 9b), the extent of all risk zone is much larger compared to the FEMA 100-year flood. For this scenario, the risk zone increased in the urbanized area and agricultural lands. Similarly, the wetlands were in a severe risk zone, whereas agricultural lands were in a low to high risk zone. More urbanized areas are located in the low risk zone, which includes residential, industrial, and road networks, which was previously in the no risk zone for the FEMA 100-year flood event. Hence, the increase in low risk extent was higher for future scenarios, which suggests an increase in a potential threat to human settlement in the future. Due to this, there can be an increase in future streamflow that may lead to enlarged flood risk areas. It is necessary to analyze the risk for future and existing 100-year flood events since the events have a higher frequency in history and are likely to happen frequently in the future as well. Moreover, analyzing the future risk would indicate the relative change in socio-economic impact in the study area with the change in the flood hazard area.

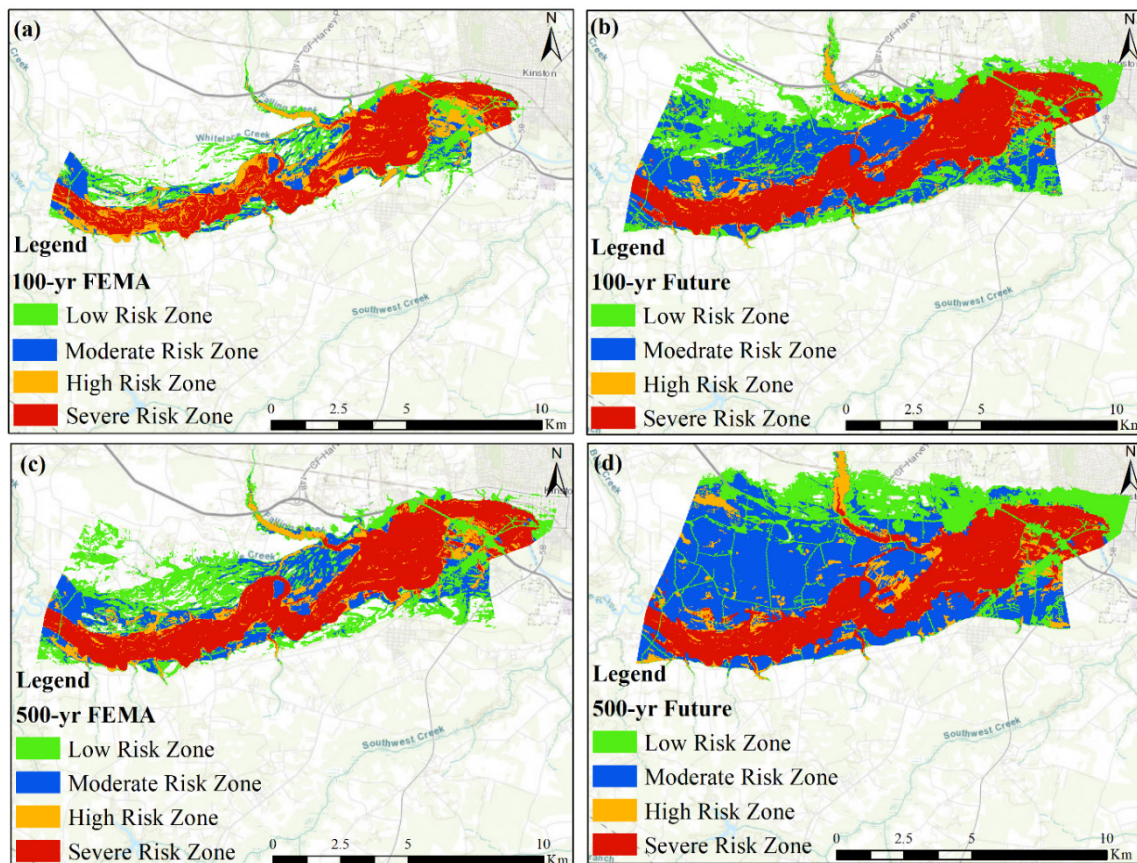


Figure 9. Floodplain mapping based on the risk zone analysis utilizing different flooding scenarios, i.e., FEMA and Future, respectively, for (a,b) 100-year and (c,d) 500-year return period flood events. Source: Esri, HERE, Garmin, Intermap, increment P Crop., GEBCO, USGS, FAO, NPS, NRCAN, GeoBase, IGN, Kadaster NL, Ordnance Survey, Esri Japan, METI, Esri China (Hong Kong), swisstopo © OpenStreetMaps contributors, and the GIS User Community.

The risk maps of the 500-year FEMA exhibit all classification of risk zones over the study area. The severe risk zone is larger, extending from waterbodies to the forest and some agricultural lands. The high risk zone covers some parts of the forest, agriculture, and water bodies (Figure 9c). The extent of the low risk zone is greater in an agricultural area near to upstream in the study area and lesser in urban areas, including road networks downstream. As the elevation of the city increases, the risk for the FEMA 500-year flood event decreases in the urbanized area. However, low-lying plain land used for farming purposes is under high risk. The 500-year future scenario results show that most of the urbanized area and agricultural lands are under the low to high risk zone (Figure 9d). Figure 9d also reveals the risk of flood zone with much of that land subjected to a higher risk zone. Future climate scenarios increase the risk that potential floods may have on the urbanized areas of this floodplain. Local water managers can make new development policies to mitigate this risk.

5. Discussion

Flooding can cause colossal damage to human life, settlement, and key infrastructures, resulting in many environmental and socio-economic consequences. The highly urbanized areas located along the floodplain can be at higher risk, even they are highly regulated [26]. Moreover, since ancient times, human populations around the globe have predominately lived near water bodies such as seashores or riverbanks to increase the ease of their living. Around 40% of the world population is currently residing within the 100 km periphery of the coastal areas, which is vulnerable to the different water-related disasters such as sea-level rises and storm surges. The consequences related to these disasters would

be more severe due to the highly concentrated population and low elevation in the coastal regions. Furthermore, due to the changes in future streamflow, flood-related hazards are likely to increase for coastal cities like Kinston. Likewise, the change in streamflow is inevitable in the future due to the sea level rises and increased global warming. Accordingly, flood protection planning ensuring minimal loss should be introduced in the future to mitigate flood risk effectively. This study utilized the streamflow projections of CMIP6 to analyze the increase in floodplain inundation due to climate change. Furthermore, different emission scenarios provided by CMIP6 were employed to evaluate the future streamflow, including different forcing level and SSP's. Hence, evaluating the future flow helps us analyze the impact of both climatic and societal change [34], allowing the acknowledgment of a broad range of future streamflow.

For the flood frequency analysis, it is important to use appropriate probability distribution that would be further used to evaluate design floods. For sub-tropical humid climatic conditions, many previous studies suggested the use of GEV as a probability distribution that will likely fit for the prediction of future streamflow [61–63]. Thus, the GEV-Max(L-Moments) was employed for the evaluation of peak flows with different year return period for both existing and future scenarios based on the fact that the climatic condition of a study reach was relevant to that of past research. Within the four different future scenarios, most of them had a DCF value greater than one while considering different return period flood events. These values suggest the future design flow is likely to be higher than the existing flows. The estimated DCF from the multimodel ensemble of four different individual future scenarios is greater than 1, based on the evaluation of the 100-year recurrence interval. The higher DCF generating scenario (SSP5-8.5) was used for this study for the convenience of analysis. For all four scenarios, the design 100-year flow would be nearly double the existing design 100-year flow. The result of the SSP5-8.5 scenario, with the higher DCF among all four scenarios, points to a higher design flow in the future than the existing condition. Moreover, as the DCF increases, the design flow also increases. The SSP5-8.5 scenario is likely to have a higher chance of flooding among all other scenarios, due to a higher predicted design flow. Hence, in further study, future scenarios for both the 100-year and 500-year return period flows were analyzed. DCM was used for the estimation of future flows of different scenarios. Then, the design streamflow from selected future scenarios was routed through the HEC-RAS 1D model for the generation of the floodplain inundation maps to compare it with the existing ones.

Since the DCF is higher for the future scenario SSP5-8.5, the increase in the future design flow is also at its maximum level. So, the maximum design flow from SSP5-8.5 scenario was then employed in the HEC-RAS model for the generation of inundation maps of the study area, Neuse River, NC. The projected future flows were compared with the existing FEMA flows to analyze the impact of climate change in future streamflow. The future 100-year flow was found to be higher than the existing 500-year flow calculated by FEMA. These results suggest an increase in flood extent in the city of Kinston and a higher possibility of a loss of public infrastructures and damage to human settlement. Previous studies suggested an increase in streamflow of the NRB, as the intensity of precipitation was projected to increase due to climatic scenarios [7,13]. For instance, in the last two decades, NC has faced more than three severe hurricanes, resulting in destructive flooding that submerged a portion of the City of Kinston. Previous studies have inferred that the impact of climate change and the change in land use can differ the result of risk analysis, due to change in the extent of floodplain [25,28]. This study uses future flows incorporating climate, land use, and socio-economic changes. Most of the population of Kinston is residing on the bank of the Neuse River, which makes the area more vulnerable to flood hazards. The agricultural land near the riverbank is running through the existing floodplain. Future flooding risks not only affecting the settlement of Kinston city but is also predicted to produce a large impact on local agricultural land, while causing loss of human life and economic harm. Thus, this study performed a zonal risk analysis based on flood hazard and land use, which has shown the severity of risk in land use. It can help local agencies to make a significant effort on

the preparedness of those areas depending on the level of risk. Also, the assessment of flood hazards, vulnerability, and risk would lead to greater mitigation of the risk of future flooding.

The current study managed to evaluate the flood hazard area as well as risk zoning so that the risk map can be prepared to depict all four risk zoning areas. Mapping can be a key factor in mitigating flood risk. Policymakers, engineers, and water resource managers can use the risk maps for the planning and constructing facilities that mitigate the risk of future flooding. The risk analysis showed the vulnerability of the community residing in the bank of the Neuse River and the fertile land on the bank of the river. Thus, appropriate research is direly needed for the analysis of future flooding in this area. In this study, different historical and future scenarios hydroclimatic data were employed to predict the future streamflow, which incorporate climatic variability in the future. The future design streamflow was used for the assessment of risk, which can be considered during the planning and building the hydraulic structures so that it can minimize the flood risk incorporated with climate change and socio-economic pathways.

6. Conclusions

This study facilitates the use of different GCMs associated with historical and future scenarios of CMIP6 to estimate the increasing flood risk caused by the changes to streamflow in the future climate. It also shows floodplain changes due to existing and future climatic scenarios. The floodplain area generated using the future climatic scenarios, SSP5-8.5, resulted in nearly two times the floodplain area that is created by existing scenarios for 100-year flood events. This shows the likelihood of an increase in flooding threats under future climate conditions. As manifested by the current change in climate, it is anticipated to increase extreme hydrological events in the future. This will subsequently increase the risk associated with these extremes. The study purposed an approach using different climatic models and observation data that can minimize the adverse impact of change in streamflow in the future. The following points summarize the main conclusion of this study:

1. Bias correction of different scenarios obtained from the multimodel ensemble with the historical data was performed using the CDF-t method. The CDF-t method increases the robustness in evaluating future change in streamflow.
2. For the estimation of the design flow, GEV-Max (L-Moments) was utilized, where SSP5-8.5 was found to have a maximum flow for the 100-year return period.
3. The DCF for most future scenarios were found to be higher than 1, suggesting the increase in future streamflow in comparison with the existing (FEMA) flow.
4. For the 100-year return period flood event, future scenario SSP5-8.5 predicted the maximum increase in the peak flow in Neuse River.
5. HEC-RAS 1D steady modeling was used to simulate the floodplain mapping extent of Neuse River, NC. The result showed a higher extent of flooding for the future 100-year scenario than for the existing FEMA 500-year peak flows.
6. Reclassification and mapping of hazard, vulnerability, and risk were completed utilizing the SSP5-8.5 scenario for the assessment of risk.
7. The extent of different flood risk zone of future flows for 100 and 500-year flood events highlights the increase in potential risk and their severity in the future.

Overall, this research highlights the use of historical and future CMIP6 climate data to forecast the future streamflow for the different return periods. The calculated streamflow is then utilized to develop the future floodplains inundation maps. Using the information from the floodplain maps, a flood risk assessment in terms of a potential threat that can be posed in the study area is performed. As evidenced by the results, the higher GHG emission scenarios are associated with intense future flooding events. These events can pose an adverse effect on the socio-economic factors of the community. On average, flood management structures last for several decades. The structures that are designed using the historic climatic information may not endure future storm events. However, the design of these

structures can be optimized by using the forecasted streamflow and by increasing sustainability for the future climatic conditions. The forecasting and risk assessment of such catastrophic events helps policymakers to prepare flood risk mitigation plans and a skeleton for making key decisions in the field of water resource management. As an alternative approach, alteration of land use can be suggested to elevate the management of flood risks sustainably.

Author Contributions: Conceptualization, A.K.; formal analysis, I.P.; M.M.R.; investigation, I.P.; M.M.R.; software, I.P.; M.M.R.; supervision, A.K.; writing—original draft, I.P.; M.M.R.; and A.K.; writing—review and editing, I.P.; M.M.R.; R.T.; and A.K. All authors have read and agreed to the published version of the manuscript.

Funding: This research received no external funding.

Acknowledgments: The authors would like to thank the three reviewers for their valuable comments. The authors are grateful to Bruce DeVantier at Southern Illinois University, Carbondale and Kenneth Lamb at Cal Poly, Pomona for providing assistance with the proofreading of the manuscript. The authors would like to express their appreciation for the support provided by the Office of the Vice-Chancellor for Research at Southern Illinois University, Carbondale. The current study was carried out using various publicly available datasets.

Conflicts of Interest: The authors declare no conflict of interest.

References

- Allen, R.M.; Dube, O.P.; Solecki, W.; Aragon-Durand, F.; Cramer, W.; Humphreys, S.; Kainuma, M.; Kala, J.; Mahowald, N.; Mulugetta, Y.; et al. Framing and context. In *Global Warming of 1.5 °C. An IPCC Special Report on the Impacts of Global Warming of 1.5 °C above Pre-Industrial Levels and Related Global Greenhouse Gas Emission Pathways, in the Context of Strengthening the Global Response to the Threat of Climate Change, Sustainable Development, and Efforts to Eradicate Poverty*; Masson-Delmotte, V.P., Zhai, H.-O., Portner, D., Roberts, J., Skea, P.R., Shukla, A., Pirani, W., Moufouma-Okia, C., Pean, R., Pidcock, S., et al., Eds.; Intergovernmental Panel on Climate Change: Geneva, Switzerland, 2018; in press.
- Merz, B.; Aerts, J.; Arnbjerg-Nielsen, K.; Baldi, M.; Becker, A.; Bichet, A.; Blöschl, G.; Bouwer, L.M.; Brauer, A.; Cioffi, F.; et al. Floods and climate: Emerging perspectives for flood risk assessment and management. *NHESS* **2014**, *14*, 1921–1942. [[CrossRef](#)]
- Easterling, D.R.; Meehl, G.A.; Parmesan, C.; Changnon, S.A.; Karl, T.R.; Mearns, L.O. Climate extremes: Observations, modeling, and impacts. *Science* **2000**, *289*, 2068–2074. [[CrossRef](#)]
- Griffin, M.T.; Montz, B.E.; Arrigo, J.S. Evaluating climate change induced water stress: A case study of the lower cape fear basin, NC. *Appl. Geogr.* **2013**, *40*, 115–128. [[CrossRef](#)]
- Middelkoop, H.; Daamen, K.; Gellens, D.; Grabs, W.; Kwadijk, J.C.; Lang, H.; Wilke, K. Impact of climate change on hydrological regimes and water resources management in the Rhine basin. *Clim. Chang.* **2001**, *49*, 105–128. [[CrossRef](#)]
- Roy, L.; Leconte, R.; Brissette, F.P.; Marche, C. The impact of climate change on seasonal floods of a southern Quebec River Basin. *Hydrol. Process.* **2001**, *15*, 3167–3179. [[CrossRef](#)]
- Arnell, N.W.; Gosling, S.N. The impacts of climate change on river flood risk at the global scale. *Clim. Chang.* **2016**, *134*, 387–401. [[CrossRef](#)]
- Hirabayashi, Y.; Kanae, S.; Emori, S.; Oki, T.; Kimoto, M. Global projections of changing risks of floods and droughts in a changing climate. *Hydrol. Sci. J.* **2008**, *53*, 754–772. [[CrossRef](#)]
- De Paola, F.; Giugni, M.; Pugliese, F.; Annis, A.; Nardi, F. GEV parameter estimation and stationary vs. non-stationary analysis of extreme rainfall in African test cities. *Hydrology* **2018**, *5*, 28. [[CrossRef](#)]
- Alfieri, L.; Feyen, L.; Dottori, F.; Bianchi, A. Ensemble flood risk assessment in Europe under high end climate scenarios. *Glob. Environ. Chang.* **2015**, *35*, 199–212. [[CrossRef](#)]
- Bhandari, R.; Kalra, A.; Kumar, S. Analyzing the effect of CMIP5 climate projections on streamflow within the Pajaro River Basin. *Water J.* **2020**, *6*, 5.
- Chattopadhyay, S.; Jha, M.K. Hydrological response due to projected climate variability in Haw River watershed, North Carolina, USA. *Hydrol. Sci. J.* **2016**, *61*, 495–506. [[CrossRef](#)]
- Johnson, T.; Butcher, J.; Deb, D.; Faizullahoy, M.; Hummel, P.; Kittle, J.; Sarkar, S. Modeling streamflow and water quality sensitivity to climate change and urban development in 20 US watersheds. *JAWRA J. Am. Water. Resour. Assoc.* **2015**, *51*, 1321–1341. [[CrossRef](#)]
- Arnell, N.W. Climate change and global water resources. *Glob. Environ. Chang.* **1999**, *9*, S31–S49. [[CrossRef](#)]

15. Hall, K. *Expected Costs of Damage from Hurricane Winds and Storm-Related Flooding*; Congressional Budget Office: Washington, DC, USA, 2019; pp. 1–48.
16. Guidance of Flood Risk Analysis and Mapping; Hydraulics: One-Dimensional Analysis. Available online: https://www.fema.gov/media-library-data/1484864685338-42d21ccf2d87c2aac95ea1d7ab6798eb/Hydraulics_OneDimensionalAnalyses_Nov_2016.pdf (accessed on 3 January 2020).
17. Brunner, G.W. *HEC-RAS, River Analysis System Hydraulic Reference Manual, Version 5.0*; US Army Corps of Engineers: Davis, CA, USA, 2016; pp. 3–538.
18. Joshi, N.; Lamichhane, G.R.; Rahaman, M.M.; Kalra, A.; Ahmad, S. *Application of HEC-RAS to Study the Sediment Transport Characteristics of Maumee River in Ohio*; World Environmental and Water Resources Congress: Reston, VA, USA, 2019; pp. 257–267.
19. Yang, J.; Townsend, R.D.; Daneshfar, B. Applying the HEC-RAS model and GIS techniques in river network floodplain delineation. *Can. J. Civil. Eng.* **2006**, *33*, 19–28. [[CrossRef](#)]
20. Lim, N.J. Performance and Uncertainty Estimation of 1-and 2-Dimensional Flood Models. Master's Thesis, University of Gävle, Gävle, Sweden, June 2011.
21. ShahiriParsa, A.; Noori, M.; Heydari, M.; Rashidi, M. Floodplain zoning simulation by using HEC-RAS and CCHE2D models in the Sungai Maka river. *Sage Open.* **2016**, *9*. [[CrossRef](#)]
22. Mehta, D.J.; Ramani, M.M.; Joshi, M.M. Application of 1-D HEC-RAS model in design of channels. *Methodology* **2013**, *1*, 4–62.
23. Peng, A.; Liu, F. Flooding simulation due to hurricane florence in North Carolina with HEC RAS. *arXiv* **2019**, arXiv:1911.09525.
24. Bathi, J.R.; Das, H.S. Vulnerability of coastal communities from storm surge and flood disasters. *Int. J. Environ. Res. Public Health* **2016**, *13*, 239. [[CrossRef](#)]
25. Tingsanchali, T.; Karim, F. Flood-hazard assessment and risk-based zoning of a tropical flood plain: Case study of the Yom River, Thailand. *Hydrol. Sci. J.* **2010**, *55*, 145–161. [[CrossRef](#)]
26. Mihiu-Pintilie, A.; Cîmpianu, C.I.; Stoleriu, C.C.; Pérez, M.N.; Paveluc, L.E. Using high-density LiDAR Data and 2D streamflow hydraulic modeling to improve urban flood hazard maps: A HEC-RAS multi-scenario approach. *Water* **2019**, *11*, 1832. [[CrossRef](#)]
27. Klijn, F.; Kreibich, H.; De Moel, H.; Penning-Rowsell, E. Adaptive flood risk management planning based on a comprehensive flood risk conceptualisation. *Mitig. Adapt. Strateg. Glob. Chang.* **2015**, *20*, 845–864. [[CrossRef](#)]
28. Tingsanchali, T.; Karim, M.F. Flood hazard and risk analysis in the southwest region of Bangladesh. *Hydrol. Process.* **2005**, *19*, 2055–2069. [[CrossRef](#)]
29. Noren, V.; Hedelin, B.; Nyberg, L.; Bishop, K. Flood risk assessment—practices in flood prone Swedish municipalities. *Int. J. Disaster. Risk Reduct.* **2016**, *18*, 206–217. [[CrossRef](#)]
30. Eyring, V.; Bony, S.; Meehl, G.A.; Senior, C.A.; Stevens, B.; Stouffer, R.J.; Taylor, K.E. Overview of the Coupled Model Intercomparison Project Phase 6 (CMIP6) experimental design and organization. *Geosci. Model Dev.* **2016**, *9*, 1937–1958. [[CrossRef](#)]
31. Meehl, G.A.; Moss, R.; Taylor, K.E.; Eyring, V.; Stouffer, R.J.; Bony, S.; Stevens, B. Climate model intercomparisons: Preparing for the next phase. *Eos Trans. Am. Geophys. Union* **2014**, *95*, 77–78. [[CrossRef](#)]
32. Riahi, K.; Van Vuuren, D.P.; Kriegler, E.; Edmonds, J.; O'Neill, B.C.; Fujimori, S.; Lutz, W. The shared socioeconomic pathways and their energy, land use, and greenhouse gas emissions implications: An overview. *Glob. Environ. Chang.* **2017**, *42*, 153–168. [[CrossRef](#)]
33. Stouffer, R.J.; Eyring, V.; Meehl, G.A.; Bony, S.; Senior, C.; Stevens, B.; Taylor, K.E. CMIP5 scientific gaps and recommendations for CMIP6. *Bull. Am. Meteorol. Soc.* **2017**, *98*, 95–105. [[CrossRef](#)]
34. O'Neill, B.C.; Tebaldi, C.; Van Vuuren, D.P.; Eyring, V.; Friedlingstein, P.; Hurtt, G.; Meehl, G.A. The scenario model intercomparison project (ScenarioMIP) for CMIP6. *Geosci. Model Dev.* **2016**, *9*, 3461–3482. [[CrossRef](#)]
35. Joshi, N.; Tamaddun, K.; Parajuli, R.; Kalra, A.; Maheshwari, P.; Mastino, L.; Velotta, M. Future changes in water supply and demand for Las Vegas valley: A system dynamic approach based on CMIP3 and CMIP5 climate projections. *Hydrology* **2020**, *7*, 16. [[CrossRef](#)]
36. Moradkhani, H.; Baird, R.G.; Wherry, S.A. Assessment of climate change impact on floodplain and hydrologic ecotones. *J. Hydrol.* **2010**, *395*, 264–278. [[CrossRef](#)]
37. Alfieri, L.; Bisselink, B.; Dottori, F.; Naumann, G.; de Roo, A.; Salamon, P.; Wyser, K.; Feyen, L. Global projections of river flood risk in a warmer world. *Earths Future* **2017**, *5*, 171–182. [[CrossRef](#)]

38. Shrestha, A.; Rahaman, M.M.; Kalra, A.; Jogineedi, R.; Maheshwari, P. Climatological drought forecasting using bias corrected CMIP6 climate data: A case study for India. *Forecasting* **2020**, *2*, 4. [[CrossRef](#)]
39. Stevenson, D.S.; Dentener, F.J.; Schultz, M.G.; Ellingsen, K.; Van Noije, T.P.C.; Wild, O.; Bergmann, D.J. Multimodel ensemble simulations of present-day and near-future tropospheric ozone. *J. Geophys. Res. Atmos.* **2006**, *111*. [[CrossRef](#)]
40. Nohara, D.; Kitoh, A.; Hosaka, M.; Oki, T. Impact of climate change on river discharge projected by multimodel ensemble. *J. Hydrometeorol.* **2006**, *7*, 1076–1089. [[CrossRef](#)]
41. Nam, D.H.; Udo, K.; Mano, A. Future fluvial flood risks in Central Vietnam assessed using global super-high-resolution climate model output. *J. Flood Risk Manag.* **2015**, *8*, 276–288. [[CrossRef](#)]
42. Kay, A.L.; Davies, H.N.; Bell, V.A.; Jones, R.G. Comparison of uncertainty sources for climate change impacts: Flood frequency in England. *Clim. Chang.* **2009**, *92*, 41–63. [[CrossRef](#)]
43. Christensen, J.H.; Boberg, F.; Christensen, O.B.; Lucas-Picher, P. On the need for bias correction of regional climate change projections of temperature and precipitation. *Geophys. Res. Lett.* **2008**, *35*. [[CrossRef](#)]
44. Nyaupane, N.; Thakur, B.; Kalra, A.; Ahmad, S. Evaluating future flood scenarios using CMIP5 climate projections. *Water* **2018**, *10*, 1866. [[CrossRef](#)]
45. Wang, L.; Chen, W. Equiratio cumulative distribution function matching as an improvement to the equidistant approach in bias correction of precipitation. *Atmos. Sci. Lett.* **2014**, *15*, 1–6. [[CrossRef](#)]
46. Salvi, K.; Kannan, S.; Ghosh, S. Statistical downscaling and bias-correction for projections of Indian rainfall and temperature in climate change studies. In Proceedings of the 4th International Conference on Environmental and Computer Science, Singapore, 2–4 September 2011; pp. 16–18.
47. Mishra, B.K.; Rafiei Emam, A.; Masago, Y.; Kumar, P.; Regmi, R.K.; Fukushi, K. Assessment of future flood inundations under climate and land use change scenarios in the Ciliwung River Basin, Jakarta. *J. Flood Risk Manag.* **2018**, *11*, S1105–S1115. [[CrossRef](#)]
48. Cannon, A.J.; Sobie, S.R.; Murdock, T.Q. Bias correction of GCM precipitation by quantile mapping: How well do methods preserve changes in quantiles and extremes? *J. Clim.* **2015**, *28*, 6938–6959. [[CrossRef](#)]
49. Camici, S.; Brocca, L.; Melone, F.; Moramarco, T. Impact of climate change on flood frequency using different climate models and downscaling approaches. *J. Hydrol. Eng.* **2014**, *19*, 04014002. [[CrossRef](#)]
50. Guo, L.Y.; Gao, Q.; Jiang, Z.H.; Li, L. Bias correction and projection of surface air temperature in LMDZ multiple simulation over central and eastern China. *Adv. Clim. Chang. Res.* **2018**, *9*, 81–92. [[CrossRef](#)]
51. Michelangeli, P.A.; Vrac, M.; Loukos, H. Probabilistic downscaling approaches: Application to wind cumulative distribution functions. *Geophys. Res. Lett.* **2009**, *36*. [[CrossRef](#)]
52. Pierce, D.W.; Cayan, D.R.; Maurer, E.P.; Abatzoglou, J.T.; Hegewisch, K.C. Improved bias correction techniques for hydrological simulations of climate change. *J. Hydrometeorol.* **2015**, *16*, 2421–2442. [[CrossRef](#)]
53. Famien, A.M.; Janicot, S.; Ochou, A.D.; Vrac, M.; Defrance, D.; Sultan, B.; Noel, T. A bias-corrected CMIP5 dataset for Africa using the CDF-t method: A contribution to agricultural impact studies. *Earth Syst. Dynam.* **2018**, *9*, 313–338. [[CrossRef](#)]
54. Yuan, X.; Wood, E.F. Downscaling precipitation or bias-correcting streamflow? Some implications for coupled general circulation model (CGCM)-based ensemble seasonal hydrologic forecast. *Water Resour. Res.* **2012**, *48*. [[CrossRef](#)]
55. Hamzah, F.M.; Yusoff, S.H.M.; Jaafar, O. L-moment-based frequency analysis of high-flow at Sungai Langat, Kajang, Selangor, Malaysia. *Sains Malays.* **2019**, *48*, 1357–1366. [[CrossRef](#)]
56. Teegavarapu, R.S.; Pathak, C.S. Statistical analysis of precipitation extremes. In *Statistical Analysis of Hydrologic Variables: Methods and Applications*; American Society of Civil Engineering: Reston, VA, USA, 2019; pp. 5–70.
57. Ayuketang Arreyndip, N.; Joseph, E. Generalized extreme value distribution models for the assessment of seasonal wind energy potential of Debuncha, Cameroon. *J. Renew. Energy* **2016**, *2016*, 9. [[CrossRef](#)]
58. Hosking, J.R.M.; Wallis, J.R.; Wood, E.F. Estimation of the generalized extreme-value distribution by the method of probability-weighted moments. *Technometrics* **1985**, *27*, 251–261. [[CrossRef](#)]
59. Santos, E.B.; Lucio, P.S.; e Silva, C.M.S. Estimating return periods for daily precipitation extreme events over the Brazilian Amazon. *Theor. Appl. Climatol.* **2016**, *126*, 585–595. [[CrossRef](#)]
60. Hosking, J.R. L-moments: Analysis and estimation of distributions using linear combinations of order statistics. *J. R. Stat. Soc. Ser. B* **1990**, *52*, 105–124. [[CrossRef](#)]
61. Hosking, J.R.M.; Wallis, J.R. L-moments. In *Regional Frequency Analysis: An Approach Based on L-Moments*; Cambridge University Press: Cambridge, UK, 2005; pp. 14–41.

62. Re, M.; Barros, V.R. Extreme rainfalls in se South America. *Clim. Chang.* **2009**, *96*, 119–136. [CrossRef]
63. Shi, P.; Chen, X.; Qu, S.M.; Zhang, Z.C.; Ma, J.L. Regional frequency analysis of low flow based on L moments: Case study in Karst area, Southwest China. *J. Hydrol. Eng.* **2010**, *15*, 370–377.
64. Kasiviswanathan, K.S.; He, J.; Tay, J.H. Flood frequency analysis using multi-objective optimization based interval estimation approach. *J. Hydrol.* **2017**, *545*, 251–262. [CrossRef]
65. NEUSE: River of Peace. Available online: <https://www.americanrivers:river/neuse-river/> (accessed on 9 December 2019).
66. Neuse River. Available online: <https://www.britannica.com/place/Neuse-River> (accessed on 9 December 2019).
67. US Climate Data. Available online: <https://www.usclimatedata.com/climate/kinston/north-carolina/united-states/usnc0359> (accessed on 9 December 2019).
68. Stewart, S.R.; Berg, R. *National Hurricane Center Tropical Cyclone Report Hurricane Florence (AL062018)*; National Hurricane Centre: Miami, FL, USA, 2019; pp. 2–98.
69. Flood Insurance Study: A Report of Hazard in Lenoir County, North Carolina and Incorporated Areas. Available online: https://fris.nc.gov/FRIS_WS/PDF/5e19eaf2b15b4aefa17344e46a19c500.pdf (accessed on 25 November 2019).
70. World Research Climate Programme. Available online: <https://esgf-node.llnl.gov/search/cmip6/> (accessed on 5 November 2019).
71. Saksena, S.; Merwade, V. Incorporating the effect of DEM resolution and accuracy for improved flood inundation mapping. *J. Hydrol.* **2015**, *530*, 180–194. [CrossRef]
72. Multi-Resolution Land Characteristics (MRLC) Consortium. Available online: <https://www.mrlc.gov/> (accessed on 22 November 2019).
73. Sillmann, J.; Kharin, V.V.; Zwiers, F.W.; Zhang, X.; Bronaugh, D. Climate extremes indices in the CMIP5 multimodel ensemble: Part 2. Future climate projections. *J. Geophys. Res. Atmos.* **2013**, *118*, 2473–2493. [CrossRef]
74. Joshi, N.; Bista, A.; Pokhrel, I.; Kalra, A.; Ahmad, S. Rainfall-Runoff Simulation in Cache River Basin, Illinois, Using HEC-HMS. In Proceedings of the World Environmental and Water Resources Congress: Watershed Management, Irrigation and Drainage, and Water Resource Planning and Management, Pittsburgh, PA, USA, 19–23 May 2019; American Society of Civil Engineers: Reston, VA, USA, 2019; pp. 348–360. [CrossRef]



© 2020 by the authors. Licensee MDPI, Basel, Switzerland. This article is an open access article distributed under the terms and conditions of the Creative Commons Attribution (CC BY) license (<http://creativecommons.org/licenses/by/4.0/>).